Soft Matter

Dynamic Article Links ►

Cite this: DOI: 10.1039/c0xx00000x

www.rsc.org/xxxxxx

ARTICLE

Dynamic self-organization and polymorphism of microtubule assembly through active interactions with kinesin

Yoshiki Tamura[a], Ryuzo Kawamura[a,‡], Kazuhiro Shikinaka[a,§], Akira Kakugo[*b,c], Yoshihito Osada[a,‡], Jian Ping Gong[b] and Hiroyuki Mayama[d]

Received (in XXX, XXX) Xth XXXXXXXXX 20XX, Accepted Xth XXXXXXXXX 20XX
DOI: 10.1039/b000000x

Abstract

In this study, we show that the energy-dissipative active self-assembly of microtubules (MTs) via a kinesin-based motility system produces various MT assemblies such as bundle-, network-, and ring-shaped structures depending on the initial conditions. Structural polymorphism of the MT assembly is depicted through phase diagrams, and morphogenesis of the MT assembly is discussed based on the following factors; binding force between MTs and motility-driving force from kinesins. This study provides new insights into the energy-dissipative dynamic self-organization of biological systems.

Keywords

Microtubules; active self-assembly; bottom-up approach

Introduction

Cytoskeletal proteins such as actins and microtubules and their motor proteins, *i.e.* myosins and kinesins, are known to play important roles in the formation of cellular shapes.[1–4] It has been demonstrated that isolated actins and microtubules can be self-organized into structures with specific patterns such as asters, networks, rings, and so on, associating with their motor proteins.[5–9] Other efforts have been also made to integrate cytoskeletal proteins into an ordered structure to exploit more complex functions in vitro, as observed in nature.[10, 11] In a previous paper, we reported that large linear-shaped actin bundles with preferential polarity, which consist of several tens of filament actin (F-actin) moieties, could be obtained through electrostatic interaction with synthetic polymers carrying positive charges.[12] In the presence of ATP, these bundles exhibit motility on a surface coated with myosin. It has been also demonstrated that some actin bundles exhibit not only translational motion along their filaments axis but also a higher sliding velocity than that of a single actin filament.[13]

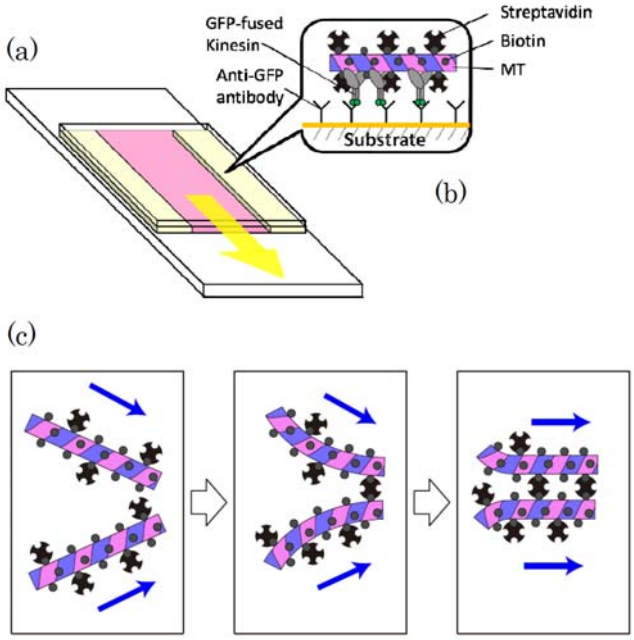

Figure 1. Schematic illustration of the preparative procedures for the active assembly of MTs. (a) Dimension of the flow cell and illustration of the MT driven on the kinesins coated on the glass surface. (b) Illustration of the MT driven on the kinesins coated on the glass surface. (c) Illustration of AcSA of MTs.

Recently, to quest more complex assemblies, a method to integrate MTs into a bundle structure on a kinesin-coated surface has been developed by employing a streptavidin (St)-biotin (Bt) interaction during the sliding motion of MTs in the presence of ATP.[6] Figure 1 shows a schematic illustration of the MT assembly process where MTs driven by the chemical energy of ATP are cross-linked through St-Bt interactions during the sliding motion on the kinesin-fixed surface. This ATP-driven, energy-

[a] *Department of Biological Science, Graduate School of Science, Hokkaido University, Sapporo 060-0810, Japan.*
[b] *Faculty of Advanced Life Science, Graduate School of Science, Hokkaido University, Sapporo 060-0810, Japan. Fax: +81-11-706-4815; Tel: +81-11-706-4815; E-mail: kakugo@sci.hokudai.ac.jp*
[c] *PRESTO, Japan Science and Technology Agency, Sapporo 060-0810, Japan.*
[d] *PRESTO, Japan Science and Technology Agency, Sapporo 060-0810, Japan.*
[‡] *Present address: Riken, Saitama 351-0198, Japan.*
[§] *Present address: Graduate School of Engineering, Tokyo University of Agriculture and Technology, Koganei 184-8588, Japan.*
† Electronic Supplementary Information (ESI) available: [Supplementary Information of supporting resutls is provided in PDF format including movies]. See DOI: 10.1039/b000000x/

dissipative self-assembly process was termed as an active self-assembly (AcSA) process and AcSA is different from a conventional self-assembly process that occurs towards the thermodynamic equilibrium without any external energy supply. Therefore, we termed the latter as a passive self-assembly (PaSA) process.[14] Indeed, AcSA process has been widely and intensively studied to obtain new insights into emergent properties found in living cells.[15, 16] Previously, we reported ring-shaped MT bundles with a diameter ranging from a submicrometer to several tens of micrometers obtained through AcSA. Semiflexible polymers including filamentous actin and DNA are also known to form ring-shaped assemblies.[17, 18] Interestingly, the ring-shaped MT assembly formed through AcSA process exhibits a preferential rotation in the counterclockwise (CCW) direction on a kinesin-coated surface depending on the number of protofilaments.[19] Thus, AcSA has great potential to facilitate various motor protein assemblies in terms of the sizes, shapes, and properties of motion. In this study, we systematically studied the effects of initial conditions such as the Bt to tubulin (Tub) ratio, St/Bt ratio, and Tub concentration (C_{Tub}) that may strongly influence the morphology of the MT assembly produced through the AcSA process. The phase diagrams of the MT assembly with structural polymorphism, including bundle-, network-, and ring-shaped structures in the Bt/Tub–C_{Tub} and St/Bt–C_{Tub} systems, are presented, and structural polymorphism is discussed on the basis of the driving force from kinesins, binding force between MTs via St-Bt interactions, and steric hindrance of St. These results may widen the designs for biodevices and biomachines with preferential motion in a bottom-up manner.

Results and Discussion

Effect of St/Bt modification on motility of MT

The AcSA process requires the motility of the MTs. Because it was considered that the high molecular weight of St might prevent MTs from binding to kinesins because of steric hindrance, we first investigated the effect of the modification ratio of St / Bt on the motility of individual MTs keeping the Bt/Tub at 1/1. Consequently, the velocity of the MTs were obtained as 0.129, 0.059, 0.054 and 0.045 μm/s for the St/Bt ratio of 0, 1/64, 1/16 and 1 respectively (see also Supplementary Information; Figure S1). Thus, MT velocity was slightly decreased with the increase of the St/Bt ratio and this suggested that the total driving force exerted on MTs should be decreased due to the reduced interaction of MTs with kinesins. Fixing the St/Bt ratio at 1/2, we also investigated the effect of Bt/Tub on the motility of MTs. On changing the Bt/Tub ratio from 1/64 to 1/1, MTs velocity was found to lie in the range of 0.03~0.05 μm/s, without showing any regular change. It was reported that the bond rupture force loaded on St-Bt interaction increased with the velocity and thus it seems that the velocities of the MTs also affect the pattern formation in the MT assemblies[20] However, the velocity of the St and Bt labeled MTs varied within a very narrow range and hence the effect of the change in velocity of MTs on pattern formation could be considered almost negligible. The velocity of MTs without St and Bt modification was found to be ~ 0.38 μm/s, which was comparable to that reported in the literature indicating that modification of MTs by St and Bt affected their motion on the kinesin fixed surface.[21,22]

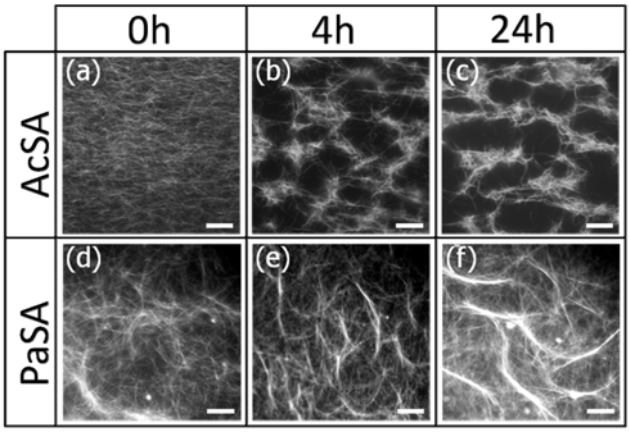

Figure 2. Time evolution of MT assembly obtained through (a–c) AcSA and (d–f) PaSA. C_{Tub} = 3360 nM, St/Bt = 1/8, and Bt/Tub = 1/1. The numbers in the figures are the time in h. Scale bar = 20 μm.

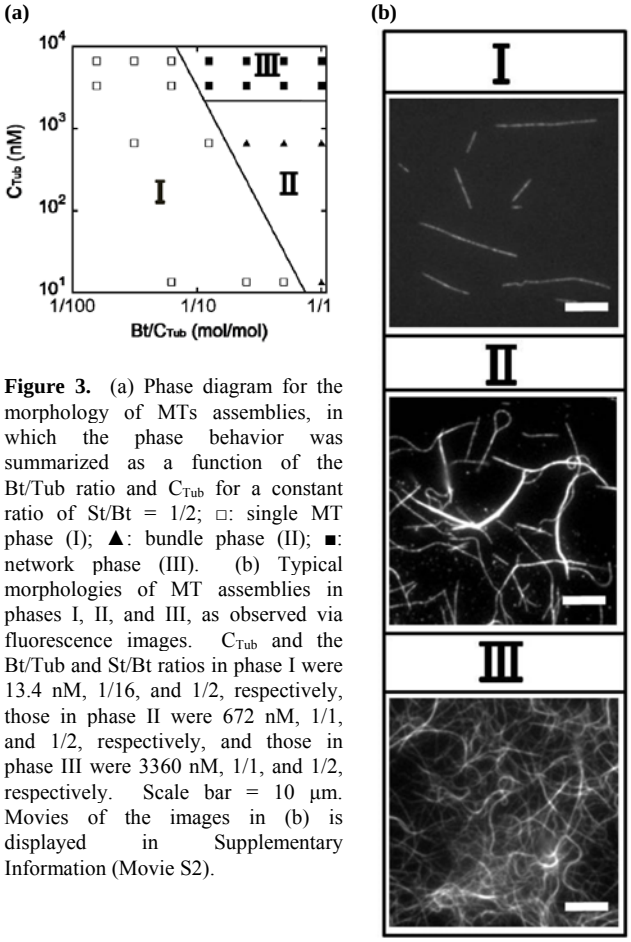

Figure 3. (a) Phase diagram for the morphology of MTs assemblies, in which the phase behavior was summarized as a function of the Bt/Tub ratio and C_{Tub} for a constant ratio of St/Bt = 1/2; □: single MT phase (I); ▲: bundle phase (II); ■: network phase (III). (b) Typical morphologies of MT assemblies in phases I, II, and III, as observed via fluorescence images. C_{Tub} and the Bt/Tub and St/Bt ratios in phase I were 13.4 nM, 1/16, and 1/2, respectively, those in phase II were 672 nM, 1/1, and 1/2, respectively, and those in phase III were 3360 nM, 1/1, and 1/2, respectively. Scale bar = 10 μm. Movies of the images in (b) is displayed in Supplementary Information (Movie S2).

Time evolution of MT assembly

Figure 2(a–c) shows a time evolution of MT assemblies obtained through AcSA (0, 4, and 24 h after ATP addition). The morphology of the MT assemblies changed with time, from a homogeneous spatial distribution to a cluster-like aggregation, while, any changes in the pattern of MTs did not occur without

ATP addition during the observation up to 24 h. After 4 h of AcSA, the morphological pattern of the MT assemblies remained essentially identical, although remodeling of the cluster-like aggregation was observed. Based on this observation, the characteristic structures of the assemblies were evaluated after 4 h of the AcSA process for preparing phase diagrams. Fig. 2(d–f) shows a time evolution of MT assemblies obtained through PaSA at 0, 4, and 24 h after mixing, without adding ATP or kinesin. As shown in this figure, aggregations of the MTs were observed just after the mixing of St (0 h). After 4 h of PaSA, thick MT bundles, which were remarkably different in morphological character from those obtained through AcSA, were formed. Growth of the MT bundles was observed even after 24 h of PaSA. This was also different from the growth observed in the AcSA system.

Effect of C_{Tub} and the Bt/Tub ratio on the structural morphology of MT assemblies

To simplify the expression for the experimental conditions, the initial C_{Tub} for AcSA was defined as the concentration of the solution that was added to the flow cell, not by the amount of fixed MTs, which requires evaluation of the number and lengths of the MTs for each condition. The concentration of the MTs was represented as the Tub monomer molar concentration. Initially, the St/Bt ratio was set at 1/2 assuming that a single St cross-links 2 Bts located on different MTs. The C_{Tub} and the Bt/Tub ratio were widely varied from 13.4 nM to 6720 nM and from 1/64 to 1/1, respectively, to achieve a variety of assembly structures. In a previous study, AcSA of the MTs was investigated only in a relatively low C_{Tub} range (9.6 – 240 nM) and the Bt/Tub ratio was fixed at 1/1.[9] As shown in Figure 3, the MT assemblies exhibited a polymorphism in a wide range of C_{Tub} and Bt/Tub ratios. There were 3 characteristic phases in the C_{Tub} and Bt/Tub phase diagram. The typical fluorescence images for the MTs assemblies in the 3 phases are shown in Figure 3(b). In phase I, MTs in the single filament state were observed. In phase II, MTs in the bundled state were preferentially formed. In this phase, bundled MTs were discriminated from single MT filaments with increasing fluorescence intensity that is more than twice of that observed in single MT. In phase III, bundled and branched MTs were observed in an overlapping manner forming a dense network; the average distances of the intersection points of MT bundles ranged from several to several tens micrometer. The ends of the MTs were found to be concealed within the network and were difficult to characterize from the images which is in contrast to the case observed in phase II. As shown in Figure 3(a), at lower C_{Tub} (13.4 nM or 672 nM), MT bundles were observed when the Bt/Tub ratio was high (II). On the other hand, at higher C_{Tub} (3360 nM or 6720 nM), the MT assemblies in a clustered network structure in which the length between MT crossing points were in a range of several to several tens micrometers was observed (III). However, when the Bt/Tub ratio was less than 1/16, cross-linked MTs were not observed even at the highest C_{Tub} (6720 nM); a filament could be recognized under the fluorescence microscope. The low cross-linking density (at low Bt/Tub ratios) and low collision frequency (at low C_{Tub}) prevent the formation of MT bundles and MT networks.

Effect of C_{Tub} and the St/Bt ratio on the structural morphology of MT assemblies

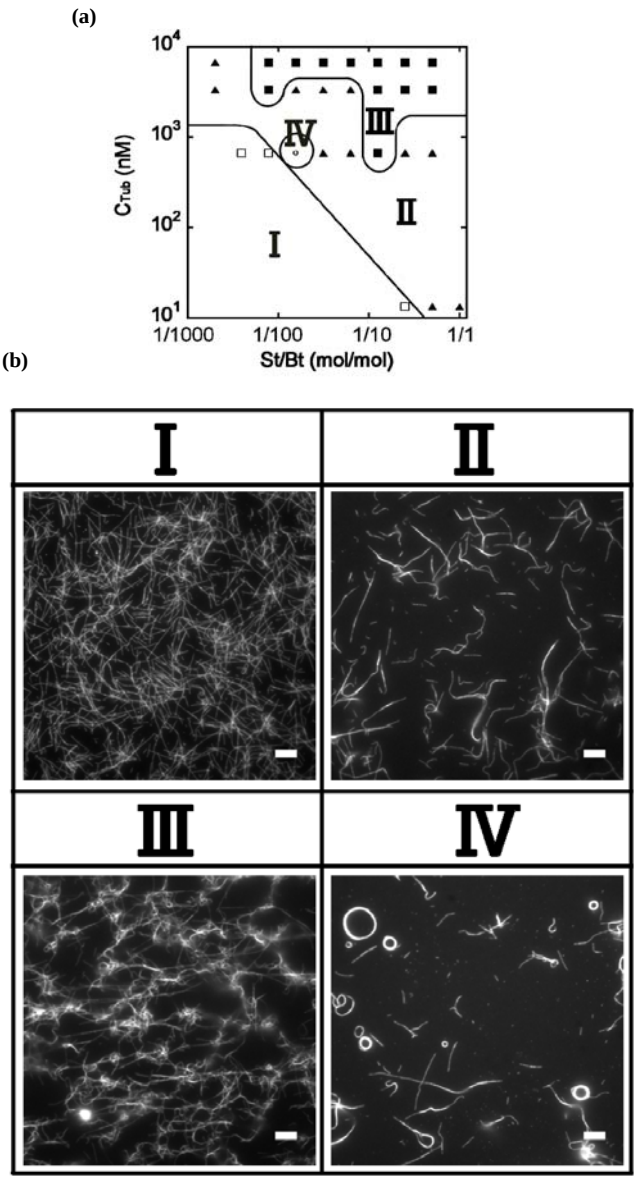

Figure 4. (a) Phase diagram for the morphology of MTs assemblies, in which the phase behavior is summarized as a function of the St/Bt ratio and C_{Tub} for constant a molar ratio of Bt/Tub = 1/1; □: single MT phase (I); ▲: bundle phase (II); ■: network phase (III); ○: ring shaped assemblies dominant (IV). (b) Typical morphologies of MT assemblies in phases I, II, III, and IV, as observed in fluorescence images. C_{Tub} and the Bt/Tub ratio were kept at constant values of 672 nM and 1/1, respectively, and the St/Bt ratios were 1/256, 1/16, 1/8, or 1/64. Scale bar = 10 μm. Movies of the images in (b) is displayed in Supplementary Information (Movie S3).

Next, we investigated the effect of C_{Tub} and the St/Bt ratio on the morphology of MT assemblies. Based on the result in the Bt/Tub ratio study, the Bt/Tub ratio was fixed at 1/1 to allow the MTs to form assemblies effectively. To study the structural variety of the MT assemblies, C_{Tub} and the St/Bt ratio were widely varied from 13.4 nM to 6720 nM and from 1/256 to 1/1, respectively. Under the experimental conditions stated above, the morphology of MTs was observed under the fluorescent microscope after 4 h of the AcSA process. The C_{Tub} and St/Bt phase diagram is shown in Figure 4(a). The typical fluorescence images of the MT assemblies are shown in Figure 4(b). When

C_{Tub} was in a lower range as 13.4 – 672 nM, the MTs existed as single filaments in the lower St/Bt region (I) and were in the bundled state in the high St/Bt region (II). When C_{Tub} was in a higher range as 3360 – 6720 nM, networks of MT assemblies were observed in the high St/Bt region (III). Similar trends were observed in the C_{Tub} and Bt/Tub phase diagram (Figure 3(a)). However, the boundary between phase II and III in the C_{Tub} and St/Bt phase diagram was complicated. A singular point (IV) where ring-shaped MTs assemblies were preferentially observed was found as shown in Figure 4(a). The point IV emerged in close vicinity to the complex boundary of phase II and III (C_{Tub} ~ 672 nM, St/Bt ~ 1/64). The diameters of the ring-shaped MT assemblies observed in this region were widely distributed (1.1 μm~13.2 μm), and the preferential rotation of those assemblies in a CCW was still preserved (CCW/clockwise (CW) = 33/7). These results agree well with those reported in a previous paper.[19, 23]

Motility of MT assembly

The MT assemblies in phase III exhibited a swarming motion, although the single MTs in phase I and MT bundles in phase II retained their translational motion. This can be attributed to the difference in the formation mechanism of MT assemblies between phases II and III. As shown in Figure 4(b), the MT density in phase III was sufficiently high to overlap. Assuming that MTs may be cross-linked via Bt-St interactions, even before AcSA begins at this C_{Tub}, it seems that MTs are cross-linked regardless of their polarity that governs the direction of the motion, *i.e.* random polarity. The components of the resultant motion vectors should be counterbalanced, and the cross-linked points may behave as nuclei for the clustered networks. Thereafter, the clusters may distribute homogeneously during AcSA. In contrast to this, MT density in phase II should not be sufficient to promote cross-linking mediated by multiple Bt and St interactions before AcSA began. Under such conditions, the MTs were preferentially bundled during AcSA. Thus, the MTs with identical polarities were exclusively integrated into bundles. The mobility of the MT assemblies in phase II is attributable to their preferential polarity in the MT alignment.[24]

Discussion of the polymorphism of MT assembly

It was considered that the factors such as binding force between MTs, driving force, and sticking that disturb the sliding motion, are responsible for the polymorphism of MT assembly. The binding force between MTs was expected to increase with increasing St/Bt ratios up to a certain optimum ratio. The ratio was presumed to be approximately 1/2, above which the binding force was diminished significantly because of occupation of the binding sites of Bts with Sts; the bundle was not formed in PaSA study (see also Supplementary information; S4). Meanwhile, the driving force exerted on MTs may decrease by increasing St/Bt ratios because of the steric hindrance of Sts and may reach a plateau after Sts fully covers the Bts on MTs. Motility of sliding MTs could be disturbed by increasing the St/Bt ratio, which results in an increased steric hindrance, being diminishing the chance of interaction among kinesins and MTs. Effects of the St/Bt ratio on these factors are illustrated in Figure 5. Here, we focus again on the C_{Tub} of 672 nM. When the St/Bt ratio was

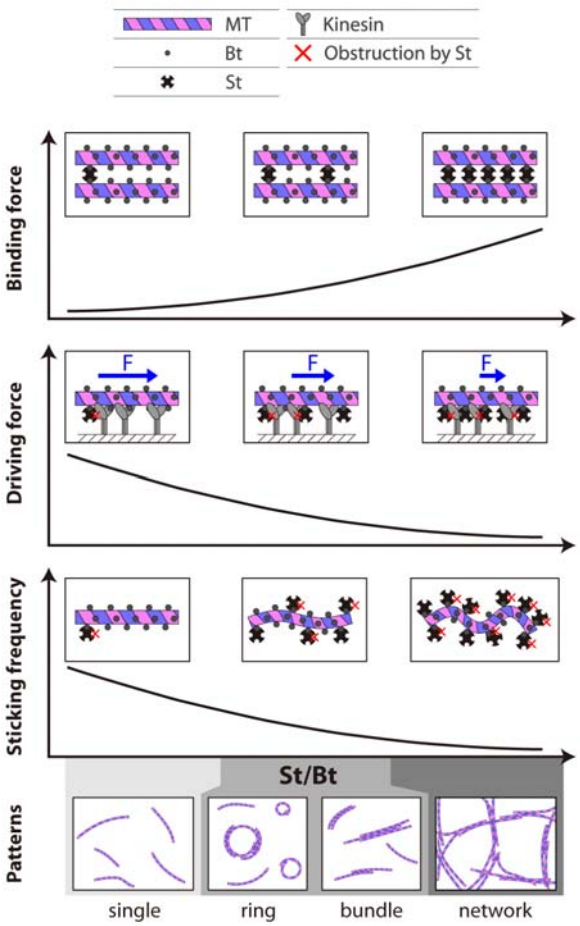

Figure 5. Predicted effects that influence the morphology of the MT assembly. (a) The effect of the St/Bt ratio on the binding force for cross-linking MTs. (b) The effect of the St/Bt ratio on the driving force exerted on the MT. (c) The sticking frequency of MTs on to kinesin coated surface, which caused by steric hindrance of St to kinesins.

smaller than 1/128, single MTs were observed. This can be attributed to the low binding force between MTs and the high driving force for dissociating the cross-linked MTs. Under such conditions, ring or bundle formation may be difficult to achieve. The ring-shaped MT assemblies observed in the bundle phase appeared between the single and network phase. In this region, large amounts of single MTs were observed at the beginning of the AcSA process. This suggests that the relatively large driving forces and moderate binding forces suppress the formation of bundle-shaped assemblies but facilitate the formation of ring-shaped assemblies, in which a configuration with intrafilament interactions is favorable. With further increases in the St/Bt ratio, the binding force increases, and the driving force simultaneously decreases. This may facilitate the interfilament cross-linking needed to form MT bundles. The bundled MTs may also suppress the formation of a ring-shaped assembly because of the increased rigidity. At the optimum St/Bt ratio, the highest cross-linking efficiency will be a trade-off between the binding and driving forces (contribution of the binding and driving forces in bundle formation is discussed later in terms of the free energy argument). Under optimum condition, MTs will be cross-linked even if there are not many cross-linking points. Therefore, cluster-like aggregations may appear in this phase (III). The optimum St/Bt ratio for network formation was determined to be approximately 1/8, which was not the stoichiometric ratio that we expected. The reaction efficiency of Sts to Bts in the flow cell

may have caused the discrepancy between the experimental and predicted ratios. Thus, the polymorphism of the MT assembly may result from the close coupling of these factors.

Conclusions

In this study, we showed that MTs were self-organized into various structures (linear, bundles, network, and rings) in response to initial conditions of C_{Tub}, St/Bt ratio, and Bt/Tub ratio through AcSA. We also showed that the ring-shaped assemblies were preferentially formed under a specific condition. These results indicated that not only the density of the MTs but also other factors such as driving force, binding force, and steric hindrance were responsible for the polymorphism of MT assembly. We expect that the present study will provide new insights into the energy-dissipative dynamic self-organization processes of biological systems. In future, the knowledge in dynamic self-organization process may also widen the range of potential applications of motor proteins in biodevices and biomachines.

Experimental

Tubulin Purification.

Tubulin was purified from porcine brain by using a high-concentration 1,4-piperazinediethanesulfonic acid (PIPES; Sigma) buffer (1 M PIPES, 20 mM EGTA, 10 mM $MgCl_2$; pH adjusted to 6.8); high-molarity PIPES buffer (HMPB) and Brinkley BR buffer 1980 (BRB80) were prepared using PIPES, and the pH was adjusted using KOH[26].

Kinesin Purification.

A GFP-fused kinesin-1 construct consisting of the first 560 amino acids (K560-GFP) was prepared, as described in previously published papers, by partially modifying the expression and purification methods as follows[22]. For the lysis of E. coli used to express K560-GFP, benzonase was added to the buffer to degrade nucleic acids. After binding the proteins to Ni-NTA resin that has affinity to the His-tag of K560-GFP, the resin was washed with a series of buffers differing in their pH value from 8.0 to 6.0 in a step-wise fashion. The target protein was eluted from the resin by washing it with the buffer containing 250 mM imidazole-Cl. The buffer of the effluent was exchanged with an MT-binding buffer [25 mM PIPES, 250 mM NaCl, 1mM EGTA, 2 mM $MgCl_2$, 0.1 mM ATP, 1mM DTT, pH 6.8 by KOH] using a PD-10 column (GE Healthcare). After the buffer exchange was finished, the K560-GFP solution was augmented with 0.5 mM GTP, 4 mM AMPPNP, 0.5 U/ml apyrase and 10 μM Paclitaxel; hereafter this composition is called the MT-binding buffer. This K560-GFP solution (2 ml) was mixed with the MT pellet obtained by the polymerization of tubulins (25 μM, 1.2ml) and subsequent ultra-centrifuge at 20,000g for 30 min (37˚C); K560-GFP was bound to MTs by incubating at 25 ˚C for 15 min. The K560-GFP bound MT was ultra-centrifuged at 300,000g for 30 min (30 ˚C) placing it on an equal volume of cushion buffer which is an MT buffer augmented with 30% (w/v) sucrose. The pellet of MTs was suspended releasing kinesins in the buffer [12 mM PIPES, 200 mM NaCl, 2 mM EGTA, 5 mM $MgCl_2$, 5 mM ATP and 10 μM Paclitaxel]. MTs were removed by ultra-centrifuge and the supernatant yielded the purified K560-GFP which was stored at –80 ˚C after snap freezing in liquid nitrogen.

Bt Labeling and Stoichiometric Estimation.

Bt-labeled Tub was prepared using biotin-XX-SE (Invitrogen) according to standard techniques[27]. The labeling stoichiometry was approximately 2 per Tub, which was estimated by spectrometric titration by using 2-(4′-hydroxyphenylazo)benzoic acid (HABA) dye (Dojindo)[28].

Rhodamine Labeling and Stoichiometric Estimation.

Rhodamine-labeled Tub was prepared using tetramethylrhodamine succinimidyl ester (TAMRA-SE; Invitrogen) according to standard techniques[29]. The ratio of rhodamine to Tub was 1/1, as determined by measuring the absorbance of the protein at 280 nm and the absorbance of tetramethylrhodamine at 555 nm.

AcSA of MTs.

Bt- and rhodamine-labeled MTs were obtained by polymerizing biotin-tubulin and rhodamine-tubulin (molar ratio, Tub : Bt : rhodamine = 1 : 1/64 : 1/10 to 1 : 1 : 1/10; final tubulin concentration, 42 μM); the solution containing the MTs was then diluted with motility buffer (80 mM PIPES, 1 mM EGTA, 2 mM $MgCl_2$, 0.5 mg mL^{-1} casein, 1 mM DTT, 4.5 mg mL^{-1} d-glucose, 50 U mL^{-1} glucose oxidase, 50 U mL^{-1} catalase, 10 μM paclitaxel, and ~1% DMSO; pH 6.8). Flow cells were prepared by placing a cover glass (18 × 18 mm^2; MATSUNAMI) on a slide glass (26 × 76 mm^2) equipped with a pair of spacers to form a chamber of approximately 4 × 18 × 0.1 mm^3 (~10 μL) (W × L × H) in dimension. A single layer of Parafilm was used to fix the spacer-separated glasses by heating. The flow cell was filled with 0.2 mg mL^{-1} anti-GFP antibody (Invitrogen) for 15 min, followed by a wash with 48 μL of casein solution (80 mM PIPES, 1 mM EGTA, 1 mM $MgCl_2$, ~0.5 mg mL^{-1} casein; pH adjusted to 6.8 using HCl). After incubating for 5 min with casein solution to mask the remaining glass surface, 24 μL of 40 nM K560-GFP solution (~80 mM PIPES, ~40 mM NaCl, 1 mM EGTA, 1 mM $MgCl_2$, 0.5 mg mL^{-1} casein, 1 mM DTT, 4.5 mg mL^{-1} d-glucose, 50 U mL^{-1} glucose oxidase, 50 U mL^{-1} catalase, 10 μM paclitaxel, ~1% DMSO; pH 6.8) were introduced and incubated for 10 min to bind the kinesins to the antibody. The flow cell was washed with 32 μL of motility buffer. A diluted solution (24 μL) of MTs (13.4 to 6720 nM in motility buffer) was then introduced and incubated for 10 min, followed by washing with 32 μL of motility buffer. A diluted solution (24 μL) of streptavidin-FITC (ST; Wako) (0 to 6720 nM in motility buffer) was then introduced and incubated for 10 min, followed by washing with 50 μL of motility buffer. Finally, AcSA was initiated by applying 24 μL of ATP solution (motility buffer supplemented with 5 mM ATP). The time of ATP addition was set as 0 h. The aforementioned experiments were performed at room temperature.

PaSA of MTs.

Bt- and rhodamine-labeled MTs diluted with the motility

buffer were mixed with streptavidin with a prescribed molar ratio of Bt/Tub at room temperature. Then, the solution of the mixture (approximately 2 μL) was placed on a slide glass using a micropipette and covered with a cover glass. The space between the slide glass and cover glass was maintained around 6 μm to allow free diffusion of MTs in the cell. Assembly of the MTs was observed at 0, 4, and 24 h after mixing MTs and Sts.

Fluorescence microscopic observation.

Rhodamine-labeled MTs in motility assays were illuminated with a 100-W mercury lamp and visualized by epifluorescence microscopy by using a PlanApo 60×/1.40 objective (Olympus). Images were captured using a cooled-CCD camera (Cascade II; Nippon Roper) connected to a PC. The motions of the MTs were analyzed using image analysis software (Image Pro Plus 5.1J; Media Cybernetics).

Acknowledgments

This research was financially supported by the Ministry of Education, Science, Sports, and Culture of Japan (Grant-in-Aid of Specially Promoted Scientific Research) and PRESTO (Japan Science and Technology Agency).

References

[1] D. J. Sharp, G. C. Rogers, J. M. Scholey, *Nature*, 2000, **407**, 41-47.
[2] T. Pollard, *Nature*, 2003, **422**, 741-745.
[3] M. L. Gardel, K. E. Kasza, C. P. Brangwynne, J. Liu, D. A. Weitz, *Methods Cell Biol.*, 2008, **89**, 487-519.
[4] J. Stricker, T. Falzone, M. L. Gardel, *J. Biomech.*, 2010, **43**, 9-14.
[5] F. J. Nédélec, T. Surrey, A. C. Maggs, S. Leibler, *Nature*, 1997, **389**, 305-308.
[6] H. Hess, J. Clemmens, C. Brunner, R. Doot, S. Luna, K. H. Ernst, V. Vogel, *Nano Lett.*, 2005, **5**, 629-633.
[7] P. Kraikivski, R. Lipowsky, J. Kierfeld, *Phys. Rev. Lett.*, 2006, **96**, 258103.
[8] V. Schaller, C. Weber, C. Semmrich, E. Frey, A. R. Bausch, *Nature*, 2010, **467**, 73-77.
[9] R. Kawamura, A. Kakugo, Y. Osada, J. P. Gong, *Nanotechnology*, 2010, **21**, 145603.
[10] T. B. Brown, W. O. Hancock, *Nano. Lett.*, 2002, **2**, 1131.
[11] W. Roos, A. Roth, E. Sackmann, J. P. Spatz, *Chem. Phys. Chem.*, 2003, **4**, 872.
[12] A. Kakugo, S. Sugimoto, J. P. Gong, Y. Osada, *Adv. Mater.*, 2002, **14**, 1124.
[13] A. Kakugo, K. Shikinaka, N. Takekawa, S. Sugimoto, Y. Osada, J. P. Gong, *Biomacromol.*, 2005, **6**, 845.
[14] G. M. Whitesides, B. Grzybowski, *Science*, 2002, **295**, 2418-2421.
[15] V. Schaller, C. Weber, C. Semmrich, E. Frey, A. R. Bausch, *Nature*, 2010, **467**, 73-77.
[16] P. Kraikivski, R. Lipowsky, J. Kierfeld, *Phys. Rev. Lett.*, 2006, **96**, 258103.
[17] L. C. Gosule, J. A. Schellman, *Nature*, 1976, **259**, 333-335.
[18] J. X. Tang, J. A. Kas, J. V. Shah, P. A. Janmey, *Eur. Biophys. J.*, 2001, **30**, 447-484.
[19] R. Kawamura, A. Kakugo, K. Shikinaka, Y. Osada, J. P. Gong, *Biomacromol.*, 2008, **9**, 2277-2282.
[20] E. Evans, *Annu. Rev. Biomol. Struct.*, 2001, **30**, 105-128.
[21] M. Tomishige, D. R. Klopfenstein, R. D. Vale, *Science*, 2002, **297**, 2263-2267.
[22] R. B. Case, D. W. Pierce, N. Hom-Booher, C. L. Hart, R. D. Vale, *Cell*, 1997, **90**, 959-966.
[23] H. Liu, E. D. Spoerke, M. Bachand, S. J. Koch, B. C. Bunker, G. D. Bachand, *Adv. Mater.*, 2008, **20**, 4476-4481.
[24] R. Kawamura, A. Kakugo, Y. Osada, J. P. Gong, *Langmuir*, 2010, **26**, 533-537.
[25] N. M.Green, *Methods Enzymol.*, 1990, **184**, 51-67.
[26] M. Castoldi, A. V. Popov, *Protein expression purif.* 2003, **32**, 83-88.
[27] A. Hyman, D. Drechsel, D. Kellogg, S. Salser, K. Sawin, P. Steffen, L. Wordeman, T. Mitchison, *Methods Enzymol.*, 1991, **196**, 478-485.
[28] N. M.Green, *Methods Enzymol.*, 1970, **18**, 418-424.
[29] J. Peloquin, Y. Komarova, G. Borisy, *Nat. Methods*, 2005, **2**, 299-303.

Table of contents entry

The energy-dissipative active self-assembly of microtubules (MTs) via a kinesin-based motility system shows various morphologies of MT assemblies depending on the initial conditions. Structural polymorphism of the MT assembly such as bundle-, network-, and ring-shaped structures is summarized to the phase diagrams.